

Relative Cooling Power Enhancement by Tuning Magneto-structural Stability in Ni-Mn-In Heusler Alloys

Jing-Han Chen,^{1, a)} Nickolaus M. Bruno,^{2, b)} Zhenhua Ning,¹ William A. Shelton,³ Ibrahim Karaman,^{4, 5} Yujin Huang,⁶ Jianguo Li,⁶ and Joseph H. Ross, Jr.^{7, 4}

¹⁾ *Department of Physics and Astronomy, Louisiana State University, Baton Rouge, Louisiana 70803, USA*

²⁾ *Department of Mechanical Engineering, South Dakota School of Mines and Technology, Rapid City, South Dakota 57701, USA*

³⁾ *Department of Chemical Engineering, Louisiana State University, Baton Rouge, Louisiana 70803, USA*

⁴⁾ *Department of Materials Science and Engineering, Texas A&M University, College Station, Texas 77843, USA*

⁵⁾ *Department of Mechanical Engineering, Texas A&M University, College Station, Texas 77843, USA*

⁶⁾ *School of Materials Science and Engineering, Shanghai Jiaotong University, Shanghai, 200240, China*

⁷⁾ *Department of Physics and Astronomy, Texas A&M University, College Station, Texas 77843, USA*

(Dated: 18 February 2019)

Off-stoichiometric Ni₂MnIn Heusler alloys have drawn recent attention due to their large magnetocaloric entropy associated with the coupled first-order magnetic and structural transformations. Here we present crystal structural, calorimetric and magnetic studies of three compositions. A significant enhancement of relative cooling power (RCP) was achieved by tuning the magnetic and structural stability through minor compositional changes, with the measured results quantitatively close to the previous prediction as a function of the ratio between the martensitic transition (T_m) temperature and austenite Curie temperature (T_C) although the maximal magnetic induced entropy (ΔS_{max}) reduction is observed in the same time. The results provided an evaluation guideline of RCPs as well as magnetic-induced entropy change in designing practical active materials.

Keywords: magnetocaloric effect, Heusler alloys, entropy, relative cooling power

I. INTRODUCTION

Materials showing the magnetocaloric effect (MCE) have been a source of growing interest because of their potential for an environmentally friendly and energy efficient refrigeration technology. Recently, many of the off-stoichiometric Heusler alloys based on Ni-Mn-Z (Z=In, Sb, Sn) have been reported to show a large MCE near room temperature^{1–8}. In particular, Ni-Mn-In type alloys have been of interest for their large MCE in the vicinity of first-order magneto-structural phase transitions, and hence potential application as a working material in magnetic refrigerators^{9,10}. Composition maps in the Ni-Mn-In system have been recently developed lending the ability to design materials^{11–13}.

Since the Ni-Mn-In Heusler alloys undergo a first-order magneto-structural phase transition, which is intimately related to the change of the long-range crystal symmetry, the crystal structures of the austenite and martensite phases have been widely investigated experimentally^{3,5,9,14–21}. It has been shown that the crystal structures of the martensite phase in Ni-Mn-In

Heusler alloys are very sensitive to chemical compositions as well as material processing while the crystal structure of austenite phase remains cubic over a wide range of composition. In this report, temperature-dependent X-ray diffraction spectra are reported. The crystal structures of both martensite and austenite are identified and connected to their magnetocaloric properties. The high-temperature austenite phase is a cubic while the low-temperature martensite phase is a 6M modulated monoclinic. The crystal structure of the modulated 6M monoclinic martensite phase can be described as the monoclinic distortion of the 3×1 supercell of the austenite phase along (1 1 0) direction. The relation of the crystal structures between the martensite and austenite phase is illustrated in Fig. 1 in case of the stoichiometric Ni₂MnIn.

One of the common physical quantities used to compare MCE materials is the relative cooling power (RCP), which represents the amount of transferred heat between hot and cold reservoirs in a magnetic refrigeration cycle^{22,23}. In a previous report¹³, we presented an analytic model, which was in good quantitative agreement with the experimental results, and predicted RCP enhancement by reducing the ratio between the martensitic transition and austenite Curie temperatures. In this paper, we prepared off-stoichiometric Ni-Mn-In based Heusler alloys with three different compositions. As the

^{a)} Electronic mail: jhchen10@lsu.edu

^{b)} Electronic mail: nickolaus.bruno@gmail.com

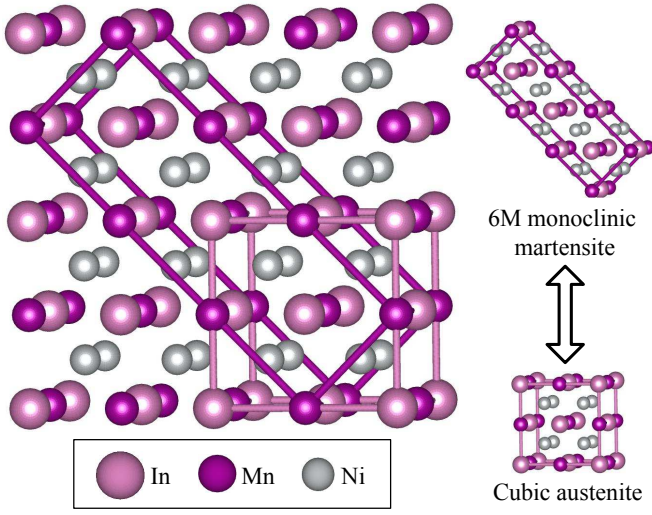


FIG. 1. 2×2 set of L_{21} stoichiometric Ni_2MnIn cubic unit cells is shown to illustrate the crystal structure of the monoclinic martensite phase as well as the cubic austenite phase. Illustration shows unit cells for both cases, with 6M structure coming from the monoclinic distortion of the cubic austenite supercell along $(1\ 1\ 0)$ direction. In this report, off-stoichiometric Ni_2MnIn samples were prepared so that the concentration ratio of Mn:In is not 1:1.

concentration of Mn increased, the strength of atomic magnetic interaction is reduced so that the magnetism of the austenite phase was modified from ferromagnetic to paramagnetic. At the same time, the martensitic structural transition temperature increased. The experimental RCPs for these materials are in a good quantitative agreement with the proposed model. By varying the ratio between martensitic transition and Curie temperature of austenite phase, we achieved a significant RCP enhancement while the maximal magnetic induced entropy change was reduced.

II. EXPERIMENTAL PROCEDURES

A. Sample Preparation

Bulk polycrystalline Ni-Mn-In alloys were prepared using arc melting in a protective high purity argon atmosphere from 99.9% pure constituents. These samples were the same preparation batches as reported previously in Refs. 12 and 13. The samples were homogenized at 900 °C for 24 hours under low pressure argon atmosphere and then quenched in room-temperature water. These heat treating conditions were found to result in single phase martensite or austenite across sharp first-order transitions as shown below.

Electron microprobe measurements were carried out using wavelength dispersive spectroscopy methods on a Cameca SX50 electron microprobe system, equipped with four wavelength-dispersive X-ray spectrometers.

The final compositions of three samples were found to be $\text{Ni}_{49.54}\text{Mn}_{36.12}\text{In}_{14.34}$ (sample A), $\text{Ni}_{49.88}\text{Mn}_{35.70}\text{In}_{14.42}$ (sample B) and $\text{Ni}_{49.53}\text{Mn}_{35.22}\text{In}_{15.22}$ (sample C), with the same labels as used in Ref. 12. The experimental results of these three samples are tabulated in Table I.

B. X-ray diffraction

Temperature-dependent high resolution powder X-ray diffraction (XRD) data were collected at the X-ray Science Division beamlines at the Advanced Photon Source, Argonne National Laboratory by using a X-ray wavelength of 0.41\AA . After grinding to powders, these samples were heat treated using the same methods as the bulk in order to relax the lattice strain due to grinding process. The temperature-dependent XRD patterns for all three samples show that they have the same martensite crystal structure and austenite crystal structure. Representative results for Sample C in the temperature region of the martensite and austenite phases are shown in Fig. 2. The signature $(1\ 1\ 1)$ reflection at $2\theta = 6.8$ degrees of the Heusler-type L_{21} order in austenite is absent in Fig. 2, which confirms the statistical disorder occupancy between Mn and In atoms. Hence we conclude the domination of cubic $B2$ structure and this is consistent with previous studies^{24,25}.

Rietveld refinements were performed using GSAS software^{26,27} and the lattice constants from the refinement are tabulated in Table II. The results in the temperature region of the martensite phase (100 K) show the 6M modulated structure (illustrated in Fig. 1, space group: $P2_1/m$), as previously reported^{14,21,28,29} while 10M and 14M modulated structures for similar compositions have also been reported^{15,17,30}. Our results indicate that the 6M martensite structure persists for samples tuned across this compositional range through which the austenite changes from ferromagnetic to paramagnetic just above the structural transition, even though the lattice contribution to the transformation entropy has been shown to undergo a large change across this range^{12,31}.

As the temperature rises, these crystal structures transform from monoclinic to cubic. We observe similar cubic lattice constants for the austenite phase (400 K) of three samples as shown in Table II. The resulting volume changes across the martensitic transition from 100 K to 400 K are also shown in Table I. These changes follow the ordering $A > B > C$, which is in line with the maximal magnetic induced entropy estimated from the specific heat shown later.

C. Magnetic Experiments and Calculation

Iso-field magnetization measurements were carried out using a Magnetic Property Measurement System (MPMS, Quantum Design) on a sample from the center of the homogenized sample plate. Figure 3 shows the

Label	WDS composition	J	$T_m(K)$	$T_C(K)$	T_m/T_C	$\Delta S_{max}(mJ/g\cdot K)$	$\Delta V/V_{100K}(\%)$
A	Ni _{49.54} Mn _{36.12} In _{14.34}	2.00	347	292	1.19	50.1	1.97
B	Ni _{49.88} Mn _{35.70} In _{14.42}	1.99	333	310	1.07	44.0	1.87
C	Ni _{49.53} Mn _{35.22} In _{15.22}	2.00	299	323	0.93	30.4	1.74

TABLE I. The corresponding experimental results of our three samples are shown. J and T_C are estimated from the high-temperature Curie-Weiss fits, and T_m (martensitic transition temperature) is defined as the maximum position of the specific heat measured while heating. The volume changes, $\Delta V = V_{400K} - V_{100K}$, are determined from the X-ray diffraction.

samples	$a(\text{\AA})$	$b(\text{\AA})$	$c(\text{\AA})$	$\beta(^{\circ})$	volume(\AA^3)
A, 100 K	4.407(7)	5.571(1)	13.000(3)	93.49(7)	13.276(8)
B, 100 K	4.408(7)	5.574(5)	13.006(6)	93.53(0)	13.294(1)
C, 100 K	4.401(7)	5.600(7)	13.006(6)	93.06(7)	13.341(4)
A, 400 K	3.002(8)	3.002(8)	3.002(8)	90.00	13.538(2)
B, 400 K	3.003(2)	3.003(2)	3.003(2)	90.00	13.543(3)
C, 400 K	3.005(5)	3.005(5)	3.005(5)	90.00	13.573(9)

TABLE II. The lattice parameters at 100 K and 400 K from the Rietveld refinement. volume in this table is defined in the unit of \AA^3 per atom. The austenite phases (i.e. 400 K) are crystallized in disorder cubic $B2$ structure (space group: $Pm\bar{3}m$) while the martensite phase (i.e. 100 K) are crystallized in 6M modulated monoclinic structure (space group: $P2_1/m$).

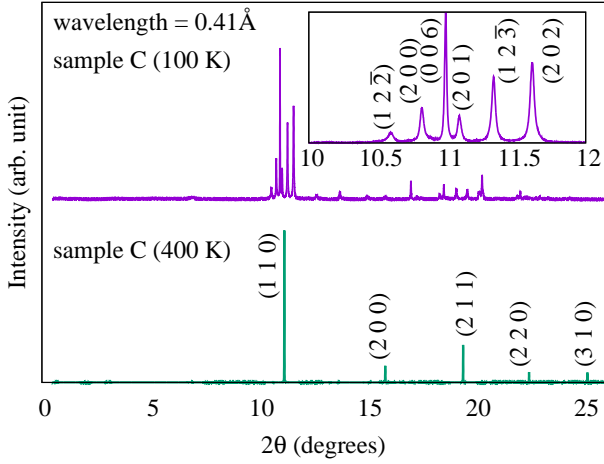


FIG. 2. X-ray diffraction at 100 K and 400 Kelvin results for the sample C are shown. The (1 1 0) intensities for all three samples are normalized to be equal to each other for comparison. The domination of cubic $B2$ structure in austenite phases is confirmed. Low temperature (martensite phase) X-ray diffraction results agree well with the reported 6M modulated structural parameters (space group: $P2_1/m$)¹⁴.

temperature-dependent magnetization in 0.05 Tesla. The transition curves, as shown, correspond to the martensitic transformation. The forward (austenite to martensite) transformation is observed on cooling the samples and the reverse transformation (martensite to austenite) is observed on sample heating. The results indicate a

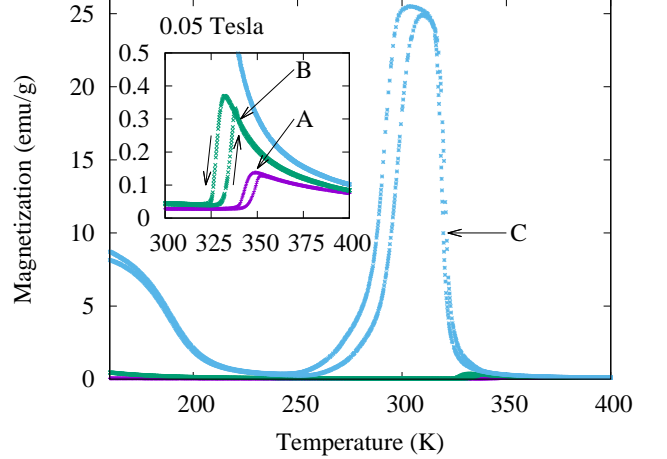


FIG. 3. Temperature dependence of the magnetization for the sample A, B and C at 0.05 T is shown. All data include results for both heating and cooling processes, as shown by arrows for sample B in the inset figure.

transition from a ferromagnetic/paramagnetic austenite to a low-magnetization martensite upon cooling. However, as we previously demonstrated in Ref. 12, the martensite phases have a relatively high degree of spin ordering (and hence reduced spin entropy) in a configuration characterized as antiferromagnetic.

The Curie-Weiss law,

$$M = n \frac{N_A}{3k_B} \mu_{eff}^2 \frac{H}{T - T_C}, \quad (1)$$

where $\mu_{eff} = g\mu_B\sqrt{J(J+1)}$, T_C is the Curie temperature and $g = 2$, was used to fit the high temperature paramagnetic magnetization curves. This fitted spin value was obtained by assuming that the density of magnetic moments (n) is identical to that of the manganese ions. The fitted results for T_C and J are listed in Table I as noted previously¹². All of these results are in agreement with a local magnetic moment of $4\mu_B$ in line with reported studies^{30,32-34} and are consistent with local magnetic moments in the sample attributed to manganese with negligible moment on other ions. It is interesting that for Ni-Co-Mn-Sn materials³⁵ the magnetism exhibits behavior much closer to itinerant magnetism, however in these materials the identical per-Mn moments point to magnetism that is very well represented as composed

of local moments on Mn ions. The order of the ratio between martensitic transition and austenite Curie temperature (T_m/T_C) is $A > B > C$ as shown in Table I.

It is worthy noting that the Curie temperature T_C decreases as the increasing of the compositional concentration of Mn, showed in Table I. To understand this behavior qualitatively, we calculated the T_C of two binary compounds MnNi and MnNi₃ by mapping energy differences onto the general Heisenberg Spin Hamiltonian within density functional theory^{36,37} using the projector augmented wave method³⁸ implemented in the Vienna ab initio simulation package^{39,40}. The generalized-gradient approximation to the exchange-correlation functional proposed by Perdew, Burke and Ernzerhof⁴¹ was used. We obtained that the T_C of MnNi was less than that of MnNi₃ which explains why T_C was decreased as the concentration of Mn atoms is increased in our materials. This gives us some insight that the magnetic exchange coupling is weakened as Mn concentration increases.

D. Entropy from Specific Heat Measurements

The absolute total entropy of the material can be estimated directly from the integration of the specific heat data

$$S(T, H = 0) = \int_0^T \frac{C_p(T', H = 0)}{T'} dT'. \quad (2)$$

Specific-heat measurements were performed using a Physical Property Measurement System (PPMS, Quantum Design). For temperatures away from the first-order martensitic transition, the conventional 2- τ method⁴² was used. For temperatures across the first-order martensitic transitions, the long heating and cooling pulses were used to guarantee the completion of the martensitic transition^{12,13}. The temperature-dependent specific heat results across the martensitic transition are shown in Fig. 4.

By utilizing Eq. 2 and the specific heat results shown in Fig. 4, the absolute total entropy close to the martensitic transition were estimated as shown in Fig. 5. Therefore, the maximal magnetic induced entropy (ΔS_{max}) was able to be determined from the entropy analysis by extending and interpolating the straight line shown in Fig. 5. The results show ΔS_{max} across the first-order martensitic transition to be $A > B > C$, which is consistent with the volume changes yielded from the X-ray diffraction data above.

Given that the lattice entropy can be approximated by the expression for the temperature region greater than the Debye temperature Θ ⁴³

$$S_L = 3R \left[\ln T - \ln \Theta + \frac{4}{3} \right] + \frac{\alpha}{K} (V - V_0), \quad (3)$$

where α is the thermal expansion and K is the compressibility. For a first-order magneto-structural transi-

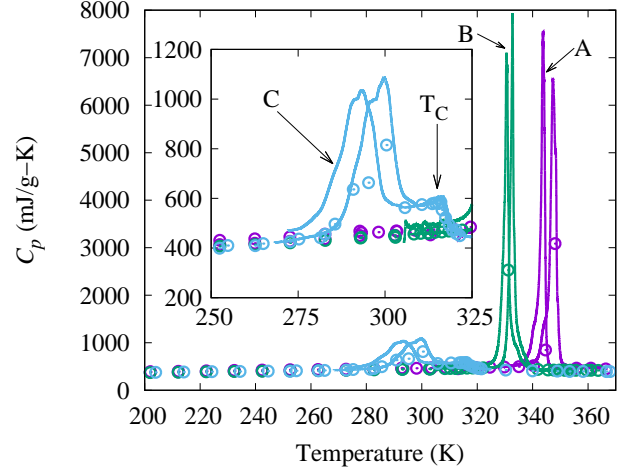


FIG. 4. Solid curves: specific heat obtained from heating and cooling measurements analyzed as described in text. Open symbols: results from the conventional 2- τ analysis, with small heat pulses, showing good agreement outside of first-order transition regime. The inset figure shows the magnification of specific heat results from sample C and its Curie temperature (T_C) is labelled.

tion, this lattice entropy is connected with the change of the Debye temperature due to the first-order structural deformation⁴³⁻⁴⁵

$$\Theta_A = \Theta_M \left(1 - \gamma \frac{\Delta V}{V} \right), \quad (4)$$

where Θ_M is the Debye temperature of the martensite phase, Θ_A is the Debye temperature of the austenite phase and γ is Grüneisen parameter. By utilizing Eq. 3 and Eq. 4, we can estimate the lattice entropy change due to the change of the Debye temperature, namely, the first term in Eq. 3. Usually, γ is between 1 and 3⁴⁶. By adopting the $\gamma = 2.405$ from the Ni-Mn-Sb alloy by the first principle⁴⁷, the resulting lattice entropy changes due to the change of Debye temperature are 4.63 mJ/g-K, 4.38 mJ/g-K and 4.04 mJ/g-K for sample A, B and C respectively. Note that the calculated lattice entropy difference among the samples is much lower than the difference of ΔS_{max} in table I. Therefore, the major ΔS_{max} difference among samples could be either from the change of thermal expansion across the martensitic transition (i.e. the second term in Eq. 3) or from the different magnetic order change across martensitic transition.

III. RELATIVE COOLING POWER

An important quantity for evaluating the performance of MCE materials is the amount of transferred heat between cold and hot reservoirs in an ideal refrigeration cycle^{48,49}. This is referred to as the relative cooling power (RCP). The estimation of the RCPs come from the inte-

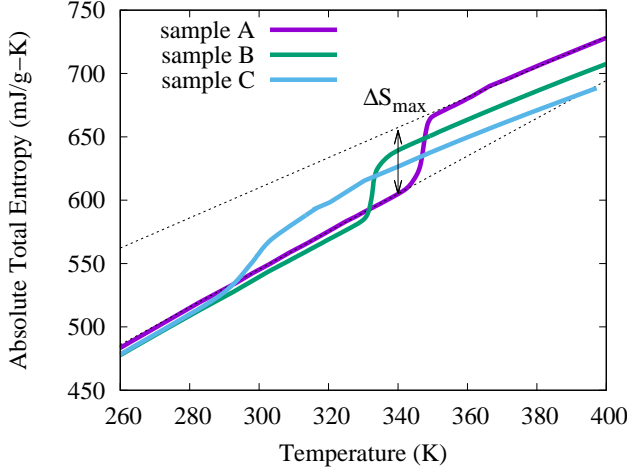


FIG. 5. The absolute entropy of sample A, B, C by Eq. 2 from the heating specific heat measurement are shown. The maximal magnetic-induced entropy ΔS_{max} of sample A is shown as a representative and the dash lines are from the linear fittings of the martensite phase entropy and austenite entropy to interpolate ΔS_{max} . The magnitude order of ΔS_{max} across martensitic transition is $A > B > C$, which is consistent with the volume changes yielded from the X-ray diffraction above.

gration of the isothermal entropy change

$$\text{RCP}(H) = \int_{T_{cold}}^{T_{hot}} \Delta S(T, 0 \rightarrow H) dT, \quad (5)$$

where T_{cold} and T_{hot} are the temperatures of the two reservoirs.

Accurate determination for the isothermal entropy change can be obtained from either specific heat in different magnetic fields⁵⁰ or field-dependent magnetization in different temperatures by the relation^{51,52},

$$\begin{aligned} \Delta S(T, 0 \rightarrow H) &= \frac{\partial}{\partial T} \left(\int_0^H M(T, H') dH' \right)_{T=const.} \\ &\cong \frac{1}{\Delta T} \left[\int_0^H M(T + \Delta T, H') dH' - \int_0^H M(T, H') dH' \right]. \end{aligned} \quad (6)$$

These two methods have proven to be in good agreement recently for Ni-Mn-In Heusler alloys given that the magnetic and calorimetric experiment were performed accurately^{13,53}.

Furthermore, Eq. 5 can be rewritten⁵² by using Eq. 6

$$\begin{aligned} \text{RCP}(H) &= \int_{T_{cold}}^{T_{hot}} \Delta S(T, 0 \rightarrow H) dT \\ &= \int_0^H M(T_{hot}, H') dH' - \int_0^H M(T_{cold}, H') dH' \end{aligned} \quad (7)$$

which indicates that RCP can be determined from isothermal magnetic measurements at only two temper-

atures without knowing the details of the magnetic entropy at points between. Thus, despite the sharp transition in this case, a larger number of magnetic isotherms (including cooling loops below the transformation) was not required for determining the RCPs.

We now consider more generally the RCP obtainable in similar alloy systems with the transformation temperature T_m closer to T_C . As we established, the austenite phases in our Ni-Mn-In materials can be described very accurately as Curie-law paramagnetic with each Mn having a spin fitted to $J = 2.0$, and ferromagnetic correlations corresponding T_C 's listed in Table I. Except for the critical region very close to T_C in small fields, this gives a good approximation for the spin polarization of samples A and B. For sample C with the structural transformation falling just below the magnetic T_C of the austenite, we extended this analysis into the ferromagnetic-ordered phase by using a mean-field description of the magnetization.

The inset of Fig. 6 shows representative spin polarization results obtained following a standard derivation with the mean spin following a Brillouin function containing the applied magnetic field enhanced by the local exchange field⁵⁴. We assumed each Mn to have a local moment with $J = 2$ and $g = 2$, coinciding with the magnetization fit. The magnetization is obtained from the average spin using the known moment per Mn, and no adjustable parameters are needed to obtain $\int M dH$, which is the integral appearing in Eq. 7. Fig. 6 shows RCP results obtained this way vs. T_m/T_C , where the temperature at which the integration is evaluated is assumed to match T_m for different compositions along the horizontal axis. In this calculation we also assumed that the martensite-phase contribution to RCP remains unchanged. In practice this term may vary in different materials, however, this term is commonly small in inverse magnetocaloric materials. The open symbols on the graph represent the RCP extracted from specific heat and magnetization for sample A, B, and C.

A good quantitative agreement between the experimental results in open symbol and our simulated solid curves are shown in Fig. 6. The predicted RCP enhancement based on the previous model has achieved by reducing T_m/T_C through varying the composition while the maximal magnetic-induced entropy of materials is actually reduced.

IV. CONCLUSION

In this study, we have prepared materials with three compositions and two of them show the only paramagnetic austenite phase while the other shows ferromagnetic austenite phase. As the Mn concentration decreases, the magnetic stability of the austenite phase is enhanced while structural stability of the martensite phase is reduced, which leads to the change of the ratio between the martensitic transition temperature and austenite Curie

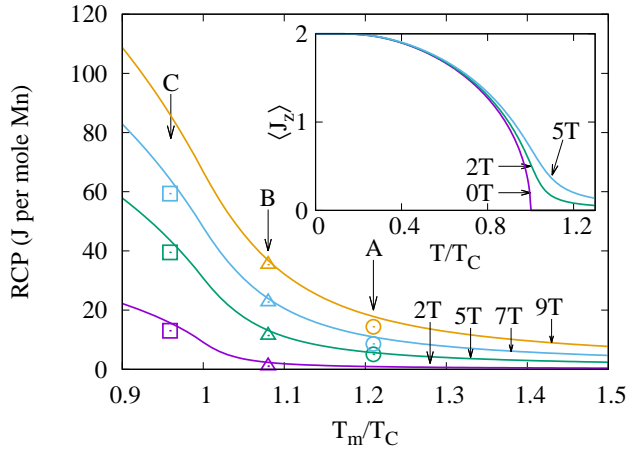


FIG. 6. Relative cooling power (in unit of J per mole Mn) vs. martensitic transformation temperature calculated for Ni-Mn-In compositions with different T_m/T_C , as described in text. Inset: computed austenite average spin moment for indicated fields.

temperature (i.e. T_m/T_C) from 1.19 to 0.93. The relative cooling power (RCP) enhancement is achieved by tuning the magneto-structural stability through reducing T_m/T_C and we confirmed the quantitative validity of the analytic RCP evaluation as a function of T_m/T_C reported previously¹². Note that the reduction of T_m/T_C ratio resulted in the enhancement of the relative cooling power but it leads to the reduction of the maximal magnetic induced entropy in the same time. Therefore, compromising consideration should be made during the design of working material for practical applications.

ACKNOWLEDGMENTS

This material is based upon work supported by the National Science Foundation under Grant No. DMR-1108396, and by the Robert A. Welch Foundation (Grant No. A-1526). This research used resources of the Advanced Photon Source, a U.S. Department of Energy (DOE) Office of Science User Facility operated for the DOE Office of Science by Argonne National Laboratory under Contract No. DE-AC02-06CH11357.

¹A. M. Tishin, Y. I. Spichkin, *The Magnetocaloric Effect and its Applications*, CRC Press, 2003.

²E. Stern-Taulats, P. O. Castillo-Villa, L. Mañosa, C. Frontera, S. Pramanick, S. Majumdar, A. Planes, Magnetocaloric effect in the low hysteresis Ni-Mn-In metamagnetic shape-memory Heusler alloy, *J. Appl. Phys.* 115 (2014) 173907.

³Y. Sutou, Y. Imano, N. Koeda, T. Omori, R. Kainuma, K. Ishida, K. Oikawa, Magnetic and martensitic transformations of NiMnX (X=In, Sn, Sb) ferromagnetic shape memory alloys, *Appl. Phys. Lett.* 85 (2004) 4358–4360.

⁴T. Krenke, E. Duman, M. Acet, E. F. Wassermann, X. Moya, L. Mañosa, A. Planes, Inverse magnetocaloric effect in ferromagnetic Ni-Mn-Sn alloys, *Nat. Mater.* 4 (2005) 450–454.

⁵K. Oikawa, W. Ito, Y. Imano, Y. Sutou, R. Kainuma, K. Ishida, S. Okamoto, O. Kitakami, T. Kanomata, Effect of magnetic field on martensitic transition of Ni₄₆Mn₄₁In₁₃ Heusler alloy, *Appl. Phys. Lett.* 88 (2006) 122507.

⁶M. Khan, N. Ali, S. Stadler, Inverse magnetocaloric effect in ferromagnetic Ni₅₀Mn_{37+x}Sb_{13-x} Heusler alloys, *J. Appl. Phys.* 101 (2007) 053919.

⁷F. S. Liu, Q. B. Wang, W. Q. Ao, Y. J. Yu, L. C. Pan, J. Q. Li, Magnetocaloric effect in high Ni content Ni₅₂Mn_{48-x}In_x alloys under low field change, *J. Magn. Magn. Mater.* 324 (2012) 514–518.

⁸L. H. Bennett, V. Provenzano, R. D. Shull, I. Levin, E. D. Torre, Y. Jin, Ferri- to ferro-magnetic transition in the martensitic phase of a Heusler alloy, *J. Alloys Compd.* 525 (2012) 34–38.

⁹T. Krenke, E. Duman, M. Acet, E. F. Wassermann, X. Moya, L. Mañosa, A. Planes, E. Suard, B. Ouladdiaf, Magnetic superelasticity and inverse magnetocaloric effect in Ni-Mn-In, *Phys. Rev. B* 75 (2007) 104414.

¹⁰Z. D. Han, D. H. Wang, C. L. Zhang, S. L. Tang, B. X. Gu, Y. W. Du, Large magnetic entropy changes in the Ni_{45.4}Mn_{41.5}In_{13.1} ferromagnetic shape memory alloy, *Appl. Phys. Lett.* 89 (2006) 182507.

¹¹Y. Huang, Q. D. Hu, J. Li, Design in Ni-Mn-In magnetic shape-memory alloy using compositional maps, *Appl. Phys. Lett.* 101 (2012) 222403.

¹²J.-H. Chen, N. M. Bruno, I. Karaman, Y. Huang, J. Li, J. H. Ross, Jr., Direct measure of giant magnetocaloric entropy contributions in Ni-Mn-In, *Acta Mater.* 105 (2016) 176–181.

¹³J.-H. Chen, N. M. Bruno, I. Karaman, Y. Huang, J. Li, J. H. Ross, Jr., Calorimetric and magnetic study for Ni₅₀Mn₃₆In₁₄ and relative cooling power in paramagnetic inverse magnetocaloric systems, *J. Appl. Phys.* 116 (2014) 203901.

¹⁴H. Yan, Y. Zhang, N. Xu, A. Senyshyn, H.-G. Brokmeier, C. Esling, X. Zhao, L. Zuo, Crystal structure determination of incommensurate modulated martensite in Ni-Mn-In Heusler alloys, *Acta Mater.* 88 (2015) 375–388.

¹⁵T. Krenke, M. Acet, E. F. Wassermann, X. Moya, L. Mañosa, A. Planes, Ferromagnetism in the austenitic and martensitic states of Ni-Mn-In alloys, *Phys. Rev. B* 73 (2006) 174413.

¹⁶B. Hernandez, J. L. S. Llamazares, J. D. Santos, M. L. Sánchez, L. Escoda, J. J. Suñol, R. Varga, C. García, J. González, Grain oriented NiMnSn and NiMnIn Heusler alloys ribbons produced by melt spinning: Martensitic transformation and magnetic properties, *J. Magn. Magn. Mater.* 321 (2009) 763–768, proceedings of the Forth Moscow International Symposium on Magnetism.

¹⁷J. L. S. Llamazares, T. Sánchez, J. D. Santos, M. J. Pérez, M. L. Sánchez, B. Hernandez, L. Escoda, J. J. Suñol, R. Varga, Martensitic phase transformation in rapidly solidified Mn₅₀Ni₄₀In₁₀ alloy ribbons, *Appl. Phys. Lett.* 92 (2008) 012513.

¹⁸A. P. Kazakov, V. N. Prudnikov, A. B. Granovsky, A. P. Zhukov, J. González, I. Dubenko, A. K. Pathak, S. Stadler, N. Ali, Direct measurements of field-induced adiabatic temperature changes near compound phase transitions in Ni-Mn-In based Heusler alloys, *Appl. Phys. Lett.* 98 (2011) 131911.

¹⁹J. Liu, N. Scheerbaum, D. Hinz, O. Gutfleisch, Magnetostructural transformation in Ni-Mn-In-Co ribbons, *Appl. Phys. Lett.* 92 (2008) 162509.

²⁰J. Liu, T. G. Woodcock, N. Scheerbaum, O. Gutfleisch, Influence of annealing on magnetic field-induced structural transformation and magnetocaloric effect in Ni-Mn-In-Co ribbons, *Acta Mater.* 57 (2009) 4911–4920.

²¹K. Abematsu, R. Y. Umetsu, R. Kainuma, T. Kanomata, K. Watanabe, K. Koyama, Structural and Magnetic Properties of Magnetic Shape Memory Alloy Ni₄₆Mn₄₁In₁₃ under Magnetic Fields, *Mater. Trans.* 55 (2014) 477–481.

²²V. K. Pecharsky, K. A. Gschneidner, Jr., Magnetocaloric effect and magnetic refrigeration, *J. Magn. Magn. Mater.* 200 (1999) 44–56.

²³V. Franco, J. S. Blázquez, B. Ingale, A. Conde, The magnetocaloric effect and magnetic refrigeration near room tempera-

- ture: materials and models, *Annu. Rev. Mater. Res.* 42 (2012) 305.
- ²⁴V. Recarte, J. I. Pérez-Landazábal, V. Sánchez-Alarcos, J. A. Rodríguez-Velamazán, Dependence of the martensitic transformation and magnetic transition on the atomic order in Ni-Mn-In metamagnetic shape memory alloys, *Acta Mater.* 60 (2012) 1937–1945.
- ²⁵N. M. Bruno, S. Wang, I. Karaman, Y. I. Chumlyakov, Reversible martensitic transformation under low magnetic fields in magnetic shape memory alloys, *Sci. Rep.* 7 (2017) 40434.
- ²⁶A. C. Larson, R. B. V. Dreele, Los Alamos National Laboratory Report LAUR (1994) 86–748.
- ²⁷B. H. Toby, *EXPGUI*, a graphical user interface for *GSAS*, *J. Appl. Cryst.* 34 (2001) 210.
- ²⁸H. E. Karaca, I. Karaman, B. Basaran, Y. Ren, Y. I. Chumlyakov, H. J. Maier, Magnetic Field-Induced Phase Transformation in NiMnCoIn Magnetic Shape-Memory Alloys - A New Actuation Mechanism with Large Work Output, *Adv. Funct. Mater.* 19 (7) (2009) 983–998.
- ²⁹W. Ito, M. Nagasako, R. Y. Umetsu, R. Kainuma, T. Kanomata, K. Ishida, Atomic ordering and magnetic properties in the $\text{Ni}_{45}\text{Co}_5\text{Mn}_{36.7}\text{In}_{13.3}$ metamagnetic shape memory alloy, *Appl. Phys. Lett.* 93 (23) (2008) 232503.
- ³⁰A. Planes, L. Mañosa, M. Acet, Magnetocaloric effect and its relation to shape-memory properties in ferromagnetic Heusler alloys, *J. Phys.* 21 (2009) 233201.
- ³¹P. J. Stonaha, M. E. Manley, N. M. Bruno, I. Karaman, R. Arroyave, N. Singh, D. L. Abernathy, S. Chi, Lattice vibrations boost demagnetization entropy in a shape-memory alloy, *Phys. Rev. B* 92 (2015) 140406.
- ³²J. Li, Z. Zhang, Y. Sun, J. Zhang, G. Zhou, H. Luo, G. Liu, The thermodynamic, electronic and magnetic properties of Ni_2MnX ($X=\text{Ge}, \text{Sn}, \text{Sb}$) Heusler alloys: a quasi-harmonic Debye model and first principles study, *Physica B* 409 (2013) 35–41.
- ³³C.-M. Li, H.-B. Luo, Q.-M. Hu, R. Yang, B. Johansson, L. Vitos, Role of magnetic and atomic ordering in the martensitic transformation of Ni-Mn-In from a first-principles study, *Phys. Rev. B* 86 (2012) 214205.
- ³⁴W. Ito, X. Xu, R. Y. Umetsu, T. Kanomata, K. Ishida, R. Kainuma, Concentration dependence of magnetic moment in $\text{Ni}_{50-x}\text{Co}_x\text{Mn}_{50-y}\text{Z}_y$ ($Z=\text{In}, \text{Sn}$) Heusler alloys, *Appl. Phys. Lett.* 97 (2010) 242512.
- ³⁵N. M. Bruno, Y. Huang, C. L. Dennis, J. Li, R. D. Shull, J. H. Ross, Jr., Y. I. Chumlyakov, I. Karaman, Effect of grain constraint on the field requirements for magnetocaloric effect in $\text{Ni}_{45}\text{Co}_5\text{Mn}_{40}\text{Sn}_{10}$ melt-spun ribbons, *J. Appl. Phys.* 120 (7) (2016) 075101.
- ³⁶P. Hohenberg, W. Kohn, Inhomogeneous electron gas, *Phys. Rev.* 136 (1964) B864–B871.
- ³⁷W. Kohn, L. J. Sham, Self-consistent equations including exchange and correlation effects, *Phys. Rev.* 140 (1965) A1133–A1138.
- ³⁸G. Kresse, D. Joubert, From ultrasoft pseudopotentials to the projector augmented-wave method, *Phys. Rev. B* 59 (1999) 1758–1775.
- ³⁹G. Kresse, J. Hafner, Ab initio molecular dynamics for liquid metals, *Phys. Rev. B* 47 (1993) 558–561.
- ⁴⁰G. Kresse, J. Furthmüller, Efficient iterative schemes for ab initio total-energy calculations using a plane-wave basis set, *Phys. Rev. B* 54 (1996) 11169–11186.
- ⁴¹J. P. Perdew, K. Burke, M. Ernzerhof, Generalized gradient approximation made simple, *Phys. Rev. Lett.* 77 (1996) 3865–3868.
- ⁴²J. S. Hwang, K. J. Lin, C. Tien, Measurement of heat capacity by fitting the whole temperature response of a heat-pulse calorimeter, *Rev. Sci. Instrum.* 68 (1997) 94–101.
- ⁴³P. J. von Ranke, N. A. de Oliveira, C. Mello, A. M. G. Carvalho, S. Gama, Analytical model to understand the colossal magnetocaloric effect, *Phys. Rev. B* 71 (2005) 054410.
- ⁴⁴G. J. Liu, J. R. Sun, J. Lin, Y. W. Xie, T. Y. Zhao, H. W. Zhang, B. G. Shen, Entropy changes due to the first-order phase transition in the $\text{Gd}_5\text{Si}_x\text{Ge}_{4-x}$ system, *Appl. Phys. Lett.* 88 (21) (2006) 212505.
- ⁴⁵B. Li, W. J. Ren, Q. Zhang, X. K. Lv, X. G. Liu, H. Meng, J. Li, D. Li, Z. D. Zhang, Magnetostructural coupling and magnetocaloric effect in Ni-Mn-In, *Appl. Phys. Lett.* 95 (17) (2009) 172506.
- ⁴⁶C. Kittel, *Introduction to Solid State Physics*, Wiley, 2004.
- ⁴⁷M. Pugaczowa-Michalska, Pressure behaviour and thermal expansion of NiMnSb from first principles calculations, *Solid State Commun.* 140 (5) (2006) 251–255.
- ⁴⁸V. K. Pecharsky, K. A. Gschneidner, Jr., Some common misconceptions concerning magnetic refrigerant materials, *J. Appl. Phys.* 90 (2001) 4614–4622.
- ⁴⁹K. A. Gschneidner, Jr., V. K. Pecharsky, A. Q. Pecharsky, C. B. Zimm, Recent developments in magnetic refrigeration, *Mater. Sci. Forum* 315 (1999) 69–76.
- ⁵⁰N. A. de Oliveira, P. J. von Ranke, Magnetocaloric effect around a magnetic phase transition, *Phys. Rev. B* 77 (2008) 214439.
- ⁵¹V. K. Pecharsky, K. A. Gschneidner, A. O. Pecharsky, A. M. Tishin, Thermodynamics of the magnetocaloric effect, *Phys. Rev. B* 64 (2001) 144406.
- ⁵²J. S. Amaral, V. S. Amaral, On estimating the magnetocaloric effect from magnetization measurements, *J. Magn. Magn. Mater.* 322 (2010) 1552–1557.
- ⁵³F. Guillou, P. Courtois, L. Porcar, P. Plandoux, D. Bourgault, V. Hardy, Calorimetric investigation of the magnetocaloric effect in $\text{Ni}_{45}\text{Co}_5\text{Mn}_{37.5}\text{In}_{12.5}$, *J. Phys. D* 45 (2012) 255001.
- ⁵⁴S. Blundell, *Magnetism in Condensed Matter*, Oxford University Press, 2001.
- ⁵⁵G. Kresse, J. Hafner, Ab initio molecular-dynamics simulation of the liquid-metal-amorphous-semiconductor transition in germanium, *Phys. Rev. B* 49 (1994) 14251–14269.